The dynamics of cluster isomerization induced by hydrogen adsorption[†]

Maite Alducin,[‡,¶] J. Iñaki Juaristi,[§,¶] Alejandra Granja-DelRío,[‖,¶] María J. López,[*,‖] and Julio A. Alonso[‖,¶]

‡ *Centro de Física de Materiales CFM/MPC (CSIC-UPV/EHU), Paseo Manuel de Lardizabal 5, 20018 Donostia-San Sebastián, Spain*

¶ *Donostia International Physics Center (DIPC), Paseo Manuel de Lardizabal 4, 20018 Donostia-San Sebastián, Spain*

§ *Departamento de Física de Materiales, Facultad de Químicas UPV/EHU, Apartado 1072, 20080 Donostia-San Sebastián, Spain*

‖ *Departamento de Física Teórica, Atómica y Óptica, Universidad de Valladolid, 47011 Valladolid, Spain*

E-mail: maria.lopez@fta.uva.es

[†]A footnote for the title

Abstract

Ab initio dynamical simulations based on the density functional formalism have been performed for molecular hydrogen impinging on a Pd_6 cluster anchored to a vacancy defect in graphene. Under the conditions assumed in the simulations, most H_2 molecules rebound after colliding with the Pd_6 cluster, but a number of molecules stay adsorbed on its surface. Depending on whether the substrate is initially at 0 or 300 K, either one third or one half of those adsorbed molecules later on dissociate on the cluster, leading to two chemisorbed H atoms. For both substrate temperatures, dissociation of H_2 triggers a transition from the original octahedral structure of the anchored Pd_6 to an incomplete pentagonal bypiramid structure, which is essentially produced by a severe elongation of the distance between two particular neighbor Pd atoms. Interestingly, no such structural change was previously observed for Pd_6 adsorbed on pristine graphene. Although this new result comes for a specific reaction –this one occurring, for instance, in the anode of hydrogen fuel cells– we anticipate that the observation of a structural change, which means that the cluster structure is not immune to the reaction taking place on its surface, can be relevant for many catalytic processes occurring on the surface of small metal particles.

Introduction

The atomic structure, as well as other properties of small clusters, usually vary with cluster size; that is, with the number of atoms in the cluster.[1,2] Apart from the ground state structure, clusters have a number of alternative isomeric structures, some of them lying within a small energy interval above the ground state. The isomeric structures are best studied by theoretical methods. Density Functional Theory (DFT),[3] combined with global optimization methods for searching structures like the basin hopping algorithm[4] or the simulated annealing method,[5] provides a helpful tool. Global optimization methods also allow studying the growth and coalescence of clusters.[6–9] Another method to investigate isomeric

structures of clusters consists in the comparison of the calculated and measured optical,[10] photoelectronic,[11] and infrared spectra.[12] Interconversion between cluster isomers may occur when heating the clusters[13] prior to melting, by encapsulation of the clusters in nanoporous materials[14] or by interaction with other species.[15]

Clusters and nanoparticles supported on appropriate substrates are used as novel catalysts in chemical reactions.[16] These nanocatalysts are characterized by strong size-dependent activity[17] as well as high size-dependent selectivity towards particular products.[18] In the catalytic processes, the reactant molecules are first adsorbed on the surface of the catalytic particles, where the occurrence of the reactions is facilitated, and the products are later desorbed. The process in which we are interested here is the adsorption of molecular hydrogen and its dissociation in atomic hydrogen on the surface of supported metal clusters. This process has interest for hydrogen fuel cells,[19] which are promising for a transportation economy based on hydrogen. An important step in the performance of the fuel cell is the dissociation of H_2 in the anode of the cell. Although dissociating H_2 in the gas phase has an energy cost of 4.52 eV, catalytic transition metal nanoparticles embedded in the porous anode facilitate H_2 dissociation.[20,21] A second issue of interest for hydrogen fuel cells is the storage of the hydrogen needed to feed the cell.[22] One of the technologies proposed to store hydrogen consists in embedding the gas in a variety of lightweight porous materials. A promising class of porous materials is the broad family of porous carbons, which have been studied intensively[23] because the inner pore's area available for hydrogen adsorption can reach high values of several thousand m^2 per gram. Although the amount of hydrogen that can be stored in pristine porous carbon materials at room temperature is not enough for the desired applications,[24] doping the material with metal clusters and nanoparticles enhances the amount of stored hydrogen. Pd is one of the best studied enhancer metals.[25–28] The mechanisms leading to that enhancement are not well known, but the dissociation of molecular hydrogen catalyzed by the metal clusters is likely to play a role in those mechanisms. Promising hydrogen sensors have been fabricated by decorating the surface of $MoS_2/SiO_2/Si$

heterojunctions with Pd nanoparticles,[29] and by coating the surface of silica microfibers with a composite material formed by Pd nanoparticles embedded in a porous poly-methyl methacrylate.[30]

How the dissociation of H_2 affects the structure of the cluster is a question of practical interest for the stability of the nanocatalytic and sensing processes mentioned above. In fact, the same question could be asked for any other reaction occurring on the surface of a metal cluster. Here we study the dissociation of H_2 on a Pd_6 cluster anchored on a graphene vacancy and focus on the changes that the structure of Pd_6 experiences as a result of that dissociation. The existence of a severe structural transformation has already been predicted from DFT calculations of the energetics of the process.[31] In this work, the structural changes are investigated by performing ab initio molecular dynamics (AIMD) simulations of the adsorption of H_2 on the supported cluster. It is crucial to understand the interplay between H_2 dissociation and the dynamics of the cluster's structural rearrangements and whether the structural changes affect the catalytic properties of the clusters.

Theoretical methods

Spin polarized AIMD simulations are performed to characterize the dynamical behavior of H_2 impinging on Pd_6 clusters anchored to a graphene vacancy (Pd_6@Gvac). The DFT code VASP,[32,33] which is based on plane waves, is used to perform total energy-conserving AIMD simulations. Exchange and correlation effects are taken into account with the generalized gradient approximation PW91 functional.[34] We use PW91 to be consistent with previous works in which we found that this GGA functional delivers good results in similar systems.[31,35–37] Only valence electrons are explicitly taken into account, and their interaction with the atomic cores is treated in the projector augmented wave (PAW) approximation[38] with the PAW potentials supplied with the VASP package.[39] The atomic cores are the $1s^2$ core for C and a Zn-like core for Pd. The electronic wave functions are expanded in a plane-

waves basis, with an energy cutoff of 400 eV, and the Brillouin zone integration is performed with a Γ-centered 2×2×1 Monkhorst–Pack grid of special **k**-points.[40] Fractional electronic-state occupancies are considered by applying the first-order Methfessel–Paxton broadening scheme, with a width of 0.1 eV.[41] Large supercells and periodic boundary conditions are used. The supercell consists in a hexagonal 5×5 graphene layer in the lateral directions. In the direction normal to the graphene layer the height of the supercell is 14 Å. The substrate is relaxed until the forces on each Pd and C atoms are below 0.02 eV/Å.

Additional static calculations have been performed with the DFT code Dacapo[42] to investigate the energy barriers associated to the structural change experienced by the supported Pd_6 cluster upon dissociation of the H_2 molecule. The static calculations used computational settings similar to those described above for the AIMD simulations except for the following ingredients: in respect to the electronic calculations, the use of ultrasoft pseudopotentials introduced by Vanderbilt,[43] a Kr-like core for the Pd atom, and an electronic temperature of 0.005 eV for the Fermi-type smearing of occupations. Finally, structure relaxations were optimized up to forces below 0.05 eV/Å. In the calculation of energy barriers we generated minimum energy paths for the structural transformation performing constrained minimizations and also using the nudge-elastic-band (NEB) methodology.[44]

The adsorption dynamics of H_2 on Pd_6@Gvac is studied in the zero pressure limit (i.e., one molecule per simulated trajectory) for normal incidence conditions and two distinct initial substrate temperatures, 0 and 300 K. The initial translational and vibrational energies of the H_2 molecule are E_i=0.125 eV and $E_{vib}(\nu=0, j=0)$=0.27 eV, respectively. The center of mass (CM) of the molecule is initially located at a height of Z=9 Å above the graphene layer, while the CM lateral position (X, Y) and molecular orientation are randomly sampled. Since we are interested in the adsorption occurring through the Pd_6 cluster, the (X, Y)-sampling is only done within half of the simulation cell, the half with triangular form that contains the Pd_6 cluster (see Fig. S1 in the Supporting Information). Using these incidence conditions we perform two sets of constant-energy AIMD simulations. In a first set of AIMD simulations,

the Pd and C atoms of the substrate are initially at rest in their equilibrium positions, that is, at T=0 K. Subsequently, the H_2 molecules impinge on the cluster and the system is allowed to evolve adiabatically at a constant total energy. In a second set of simulations, the substrate (Pd_6@Gvac) is first equilibrated at 300 K during 7 ps using the Nosé thermostat[45] implemented in VASP and a Nosé frequency of around 36 THz, appropriate to guarantee that the obtained configurations constitute a canonical ensemble. Next, we run energy-conserving AIMD simulations of H_2 impinging on the anchored cluster, in which the initial positions and velocities of the C and Pd atoms are randomly taken from the set of configurations generated during the thermalization at T=300 K. For the short simulation times of interest (4 ps in our case), this procedure, which is commonly used in gas-surface dynamics studies,[46–53] constitutes a reasonable approximation to take into account substrate temperature effects.[50] Finally, let us remark that the H_2 incidence conditions are the same we used previously to investigate the adsorption dynamics of H_2 on Pd_6 clusters supported on non-defective graphene at T=0 K.[35] Therefore, the comparison between our new and previous results will provide additional information on how the isomerization process affect the dissociation and adsorption probabilities.

Results and discussion

Insights from previous static calculations

The lowest energy geometrical configuration of an isolated Pd_6 cluster in gas phase is the octahedron (OCT).[37] This structure is maintained, with only minimal distortions, when Pd_6 is either deposited on pristine graphene or anchored on a graphene vacancy.[36] The ground state octahedral structure of Pd_6@Gvac is depicted in the top-left panel of Fig. 1. The orientation of the Pd_6 cluster is such that a triangular face of the octahedron rests directly on the graphene layer. One Pd atom of that triangular face is clearly located above the center of the vacancy, saturating the dangling bonds of the three C atoms around the

vacant site. The other two Pd atoms of that triangular face sit above C-C bonds around the vacancy. These two atoms are labelled Pd_1 and Pd_2 in Fig. 1. This triangular face is tilted with respect to the graphene plane. The three C first neighbors to the vacant site pop out from the graphene plane by about 0.5–0.7 Å in the direction to the cluster, and the C atoms of the next shell pop out by about 0.3–0.4 Å. The adsorption energy of Pd_6 on the graphene vacancy, 5.6 eV,[36] is much larger than the corresponding adsorption energy on pristine graphene, 1.1 eV.[37] The latter guaranties the high stability of the anchored Pd_6 against desorption.[36]

The Pd_6@Gvac system has a particularly interesting low-lying isomer.[31] Its structure, shown in the top-right panel of Fig. 1, is an incomplete pentagonal bipyramid (IPB) in which one of the atoms of the equatorial pentagonal plane is missing. The lower apex atom of the axis of the bipyramid saturates the graphene vacancy and the two equatorial Pd atoms neighbors of the empty site of the pentagon are attached to C–C bonds around the vacancy. The equatorial plane of the bipyramid is tilted with respect to the graphene plane. The energy of this Pd_6@Gvac IPB structure is 0.15 eV above that of the Pd_6@Gvac ground state OCT structure.[31] In the case of gas-phase Pd_6 clusters, the energy difference between the IPB and OCT structures is substantially larger, 0.29 eV.[37]

Static calculations performed in a previous work[31] revealed that upon molecular adsorption of H_2 on octahedral Pd_6 anchored to a graphene vacancy, the structure of the cluster remains unchanged. However, dissociation of the adsorbed H_2 molecule induces a structural transition in the anchored Pd_6 cluster from its OCT structure to the less symmetric IPB structure (see bottom-right panel of Fig. 1). This is, in fact, the lowest energy structure of the system. Interestingly, when Pd_6 is supported on perfect (faultless) graphene neither the adsorption of molecular H_2 nor the dissociation of the molecule induce structural changes in the Pd_6 cluster.[31,37] It is worth mentioning that Pd_6 adsorbed on pristine graphene has a spin magnetic moment of $2\mu_B$ that is completely quenched upon dissociation of H_2 on the cluster.[54] However, in the case of Pd_6@Gvac, the spin magnetic moment of the sup-

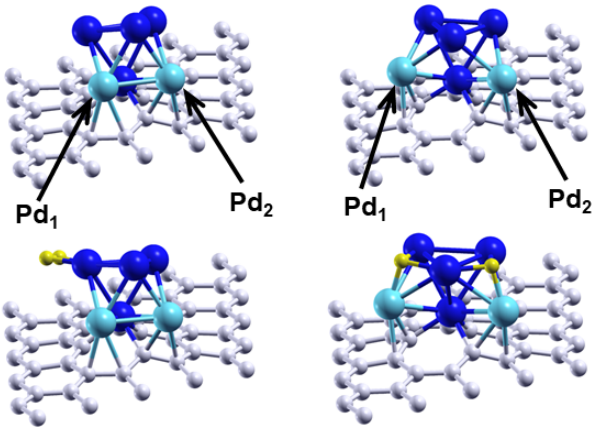

Figure 1: Top panels: The lowest energy geometrical structure (octahedron, OCT) of Pd_6 anchored on a graphene vacancy (top-left) and the incomplete pentagonal bipyramid (IPB) isomer with energy lying 0.15 eV above the OCT ground state (top-right). Blue and grey spheres represent Pd and C atoms, respectively. In the OCT structure (left), a triangular face of the the Pd_6 octahedron rests directly on the graphene plane. One Pd atom of that triangular face is located above the center of the vacancy, saturating the dangling bonds of the three C atoms around the vacant site. In the IPB structure (right), the lower apex atom of the axis of the incomplete bipyramid saturates the graphene vacancy. Bottom panels: Lowest energy structures after adsorbing H_2 (yellow spheres) on Pd_6@Gvac. The OCT structure is preserved for molecular adsorption of H_2 (bottom-left), while IPB is the ground state structure for dissociatively adsorbed H_2 (bottom-right). The light-blue atoms labelled Pd_1 and Pd_2 are used to follow the dynamics of the structural change in the AIMD simulations.

ported cluster is practically zero and it remains negligible upon the dissociative or molecular adsorption of H_2.

Dynamical simulations of the change in the cluster structure induced by H_2 dissociation

Considering the severe structural change experienced by the supported Pd_6 cluster when H_2 is dissociatively adsorbed, we find relevant to explore the dynamical aspects of that structural transition, as well as its dependence on the substrate temperature by performing AIMD simulations at two initial temperatures of the substrate, T=0 and 300 K. In particular, we want to address whether the H_2 dissociation and the structural Pd_6 rearrangement occur simultaneously or whether the two are sequential.

To this aim, one hundred constant-energy AIMD trajectories have been calculated with the substrate, Pd_6@Gvac, initially at T=0 K and a second set of one hundred AIMD trajectories with the substrate initially equilibrated at T=300 K (see Theoretical Methods). Three different outcomes can occur in the time spanned by each simulated trajectory: bouncing off the molecule, molecular adsorption on the Pd cluster, and dissociation of the molecule in two H atoms on the Pd cluster. Since we are interested in the adsorption and dissociation occurring in the low hydrogen pressure and low Pd coverage limit, any molecule exiting the (5×5) parallelogram centered at the Pd_6 cluster is considered as reflected. All the trajectories are propagated for a time of 2 ps with a time step for the integration of the dynamical equations of motion of 0.5 fs, except if H_2 dissociation is detected within the 2 ps time. In those cases, the interesting ones for the present work, the simulations have been continued until reaching a total integration time of 4 ps. In the constant-energy simulations at an initial substrate temperature T=0 K, the number of trajectories out of 100 leading to dissociative adsorption, molecular adsorption, and bouncing off are 6, 12, and 82, respectively. For the constant-energy simulations at an initial substrate temperature T=300 K, the corresponding numbers are 6, 7, and 87, respectively. The percentage of trajectories leading to dissociation of H_2 is equally small for both substrate temperatures. Excluding the bouncing off events, the rest of simulated trajectories begin with a molecular adsorption step (18 and 13 cases at T=0 K and T=300 K, respectively), although the adsorbed molecule is quite mobile on the surface of the Pd_6 cluster. Later on, one third of the adsorbing trajectories (6 out of 18) leads to dissociation at T=0 K, while about one half (6 out of 13) does it at T=300 K.

In order to analyze how the presence of defects on the carbon substrate affects the ability of Pd_6 to dissociate H_2 we have completed the statistical sampling of our previous AIMD calculations for H_2 impinging on Pd_6 supported on pristine graphene at 0 K.[35] For this purpose, we have calculated 40 additional AIMD trajectories, which added to the previous 60 amount to a total of 100 trajectories. There are six H_2 dissociation events out of the 100 trajectories. These results indicate that the H_2 dissociation probability is similar (six per

cent) irrespective of whether the Pd_6 cluster is supported on pristine or defective graphene. Nevertheless, the main difference, to be discussed in detail below, is that the transition from the OCT to the IPB structure following H_2 dissociation occurs only in the case of defective graphene. At this point, it is worth remarking that the structural transition from OCT to IPB does not occur in the absence on dissociated H_2. This conclusion arises, first of all, from the static calculations already discussed, which show that in the ground state of Pd_6@Gvac the anchored Pd_6 cluster presents the OCT structure. In addition, during the thermal equilibration dynamics of the Pd_6@Gvac substrate at T=300 K, the Pd_6 cluster always remains in its OCT structure.

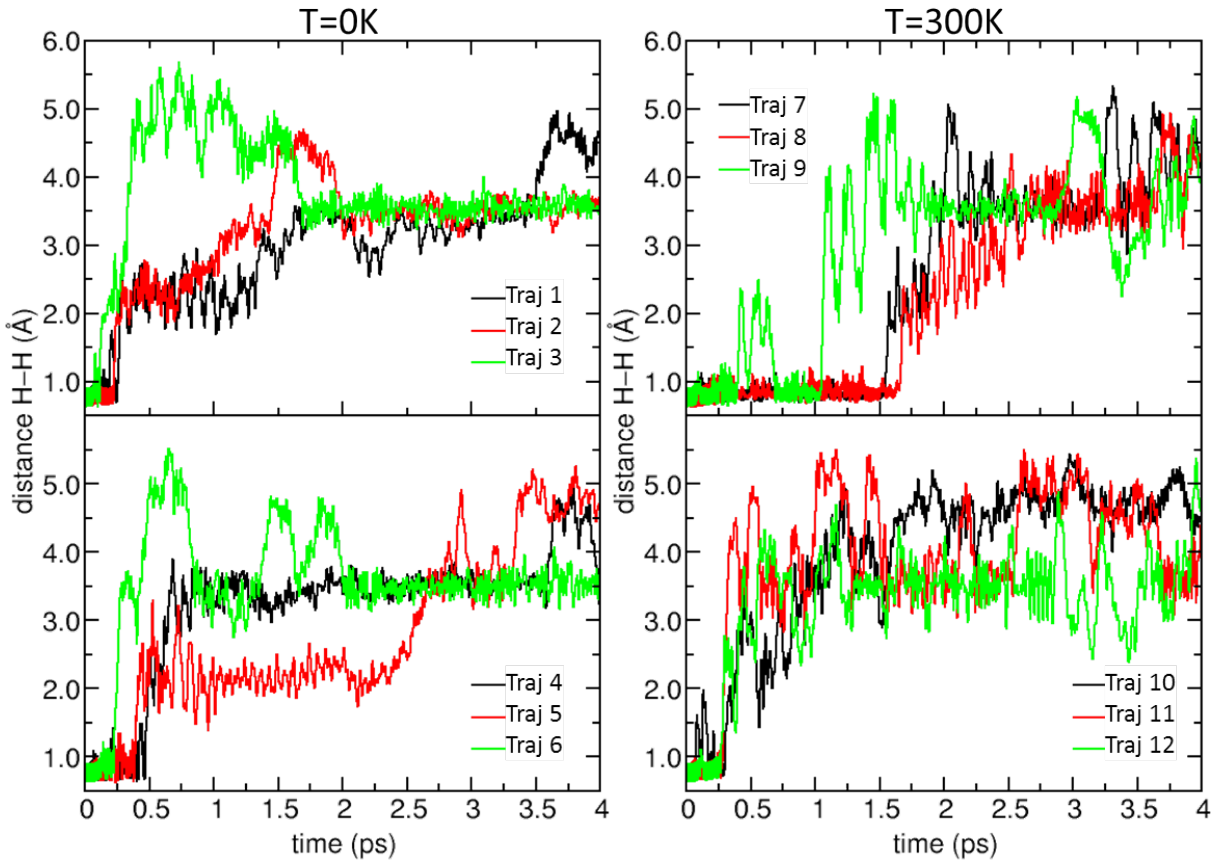

Figure 2: Distance between the two hydrogen atoms as a function of time for the trajectories leading to dissociative adsorption. The initial temperature of the substrate is T=0 K (left panel) and T=300 K (right panel). The dissociating trajectories at T=0 K are labelled from 1 to 6 and at T=300 K from 7 to 12.

Figure 2 shows the evolution of the distance d(H-H) between the two hydrogen atoms as

a function of time for each individual trajectory leading to dissociative adsorption. In the left panel of the figure, the initial temperature of the Pd_6@Gvac substrate before starting the simulations is T=0 K. Trapping of the H_2 molecules in the vicinity of the Pd_6 cluster occurs soon after the beginning of the simulations. Once trapped, the molecules move over the surface of the Pd_6 cluster for a while before dissociating, with d(H-H) oscillating around its equilibrium value of 0.75 Å. The time the molecules remain dynamically trapped without dissociating differs from one trajectory to another, but it never exceeds 500 fs. Dissociation of H_2 occurs in the lateral regions of the Pd_6 octahedron, around the triangular face which is in direct contact with the graphene layer, and is characterized by a sudden increase of d(H-H) up to values of 2 Å or larger. After dissociation, the H-H distance varies widely between different trajectories. However, in each individual trajectory the motion of each H atom is quite restricted. The distance d(H-H) shows low amplitude oscillations around an average value in some particular intervals of the simulation. The reason is that during those intervals the motions of the two H atoms are restricted to specific separated regions, mainly over two triangular faces of Pd_6, until one of the atoms moves to a different face. In contrast, in the trajectories showing molecular adsorption of H_2 with no dissociation, the molecules move on the cluster surface and the values of d(H-H) do not exceed 1.4 Å, except for some occasional excursions to larger values that later return to normal.

The right side panel of Fig. 2 shows the evolution of d(H-H) for the simulations leading to dissociative adsorption when the substrate is initially equilibrated at T=300 K. An interesting difference can be observed compared to T=0 K. At T=300 K, the time required for H_2 dissociation is widespread: it occurs in the first 500 fs, as before, in half of the cases, but it takes place at longer times, up to 1.7 ps, in the other trajectories. After dissociation, the two H atoms are more mobile compared to dissociation at T=0 K. This is due to the initial substrate temperature.

The in-depth analysis of the trajectories leading to H_2 dissociation reveals that the geometrical structure of the Pd_6 cluster changes in most cases from the initial OCT to an

IPB-like isomer. The structural transition consists in the drastic elongation of the Pd–Pd distance between two particular Pd neighbors in the equatorial plane of the octahedron (see Fig. 1). The elongation of this distance results in the breaking of the bond between these two Pd atoms. As a consequence, the two Pd–Pd–Pd angles between unbroken Pd–Pd bonds in the equatorial plane grow larger than 90°, and in this way the OCT deforms becoming an incomplete pentagonal bipyramid, that is, a bipyramid with an atom missing from the equatorial plane. To illustrate this point, Fig. 3 shows as an example several snapshots along the trajectory labelled "Traj 3" in Fig. 2. The dissociation of H_2 occurs soon after arriving at the cluster. Then, it takes a bit more than 2 ps for the structural change to occur, and the IPB isomer is visible in the snapshots at $t = 2.75$ ps and successive ones. The enlarged distance between two equatorial (adjacent) Pd atoms is quite clear.

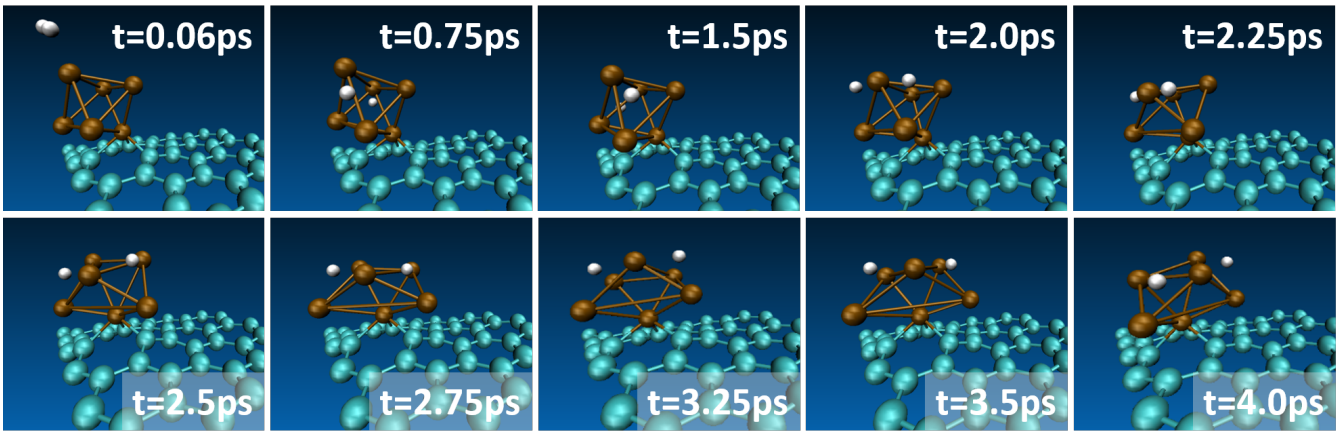

Figure 3: Typical snapshots along a representative AIMD trajectory ("Traj 3" in Fig. 2) leading first to H_2 dissociation and later on to the structural transition of the anchored Pd_6 cluster from the OCT to the IPB isomer. Plots produced with VMD software.[55] Blue, brown, and white spheres represent C, Pd, and H atoms, respectively.

Figure 4 shows the time evolution of the distance d(Pd–Pd) between the two relevant Pd atoms –denoted Pd_1 and Pd_2 in Fig. 1– along the dissociating trajectories at T=0 and 300 K. The equilibrium distance between these two atoms in the octahedron is 2.77 Å. The trajectories at T=0 K (left side panel of Fig. 4) indicate that d(Pd–Pd) oscillates irregularly as soon as H_2 is effectively trapped by the cluster. These oscillations become especially pronounced

after the molecule dissociates. All the other interatomic Pd–Pd distances also fluctuate around their initial values, although to a lower extent. Clearly, these oscillations manifest that the cluster is partially absorbing the energy liberated during the initial adsorption and subsequent dissociation of the H_2 molecule. At a substantially later time, d(Pd_1-Pd_2) undergoes a sudden elongation reaching values between 4.5 and 5.5 Å, which is the signature of the structural change. This structural transition occurs well after the instant at which H_2 dissociates, specifically, about 1.5–1.8 ps later in four simulations and about 3 ps later in one simulation. These are the time intervals required for the excitation of the Pd–Pd stretching mode leading to the OCT-IPB structural change. The evolution of the cluster structure after H_2 dissociation observed in the simulations can be summarized as follows. The octahedron undergoes a reorientation consisting in a partial rotation around the four-fold axis joining the Pd atom saturating the graphene vacancy and the Pd atom on the opposite apex. At the same time the shape of the equatorial Pd_4 plane, which is initially a square, oscillates between a rectangle with two long and two short sides and another rectangle in which the long and short sides are exchanged. Finally, one of the long sides grows significantly large and the structural transition to the IPB isomer takes place. In this process the distance between the two apex atoms (upper and lower apex) of the cluster decreases and the cluster flattens. There is a single exception at T=0 K, in which an H_2 dissociation event is not followed by the structural cluster change within the time spanned by the simulation.

The simulations at T=300 K (right side panel of Fig. 4) show that the structural change triggered by the dissociation of H_2 occurs at shorter times as compared to the simulations at T=0 K. As before, one trajectory shows no structural change after 4 ps of simulation time. Summarizing, the energy liberated when the H_2 molecule dissociates induces, in most cases, a structural transition of the anchored Pd_6 cluster from its original OCT structure to an IPB-like isomer. The obvious reason behind such transformation is that the latter is the lowest energy state of the system of two H atoms on Pd_6@Gvac. What the AIMD simulations show is that the activation barriers that separate the two structures are easily

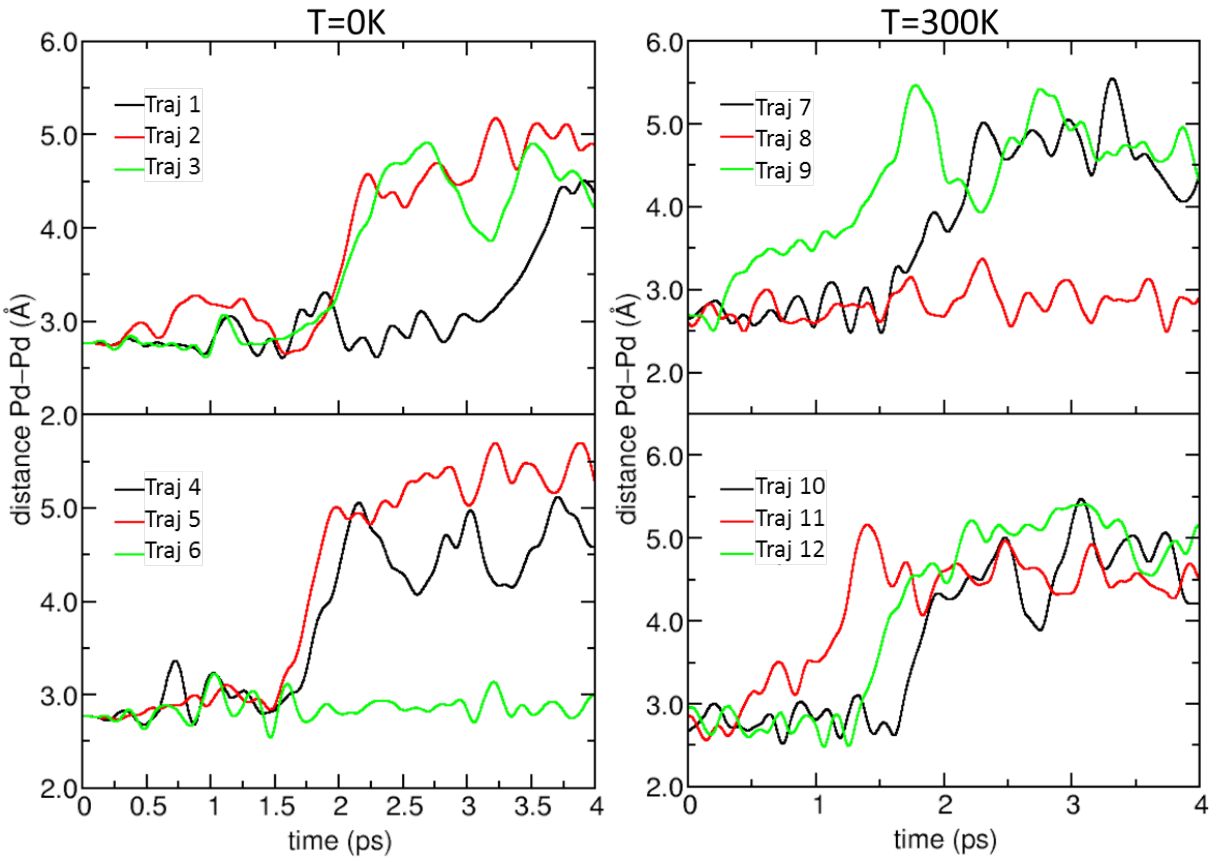

Figure 4: Distance between the Pd_1 and Pd_2 atoms (see Fig. 1) along the trajectories corresponding to dissociative adsorption of H_2. The initial temperature of the substrate before starting the simulations is T=0 K (left panel), and T=300 K (right panel). Trajectories are labelled as in Fig. 2. In each panel there is a single case in which the elongation of the Pd_1-Pd_2 distance leading to the structural transition does not occur.

surpassed. Although the isomerization has been exhibited here for the case of anchored Pd_6, the possibility of similar structural transitions, and how this affects the catalytic processes or other properties, should be considered in general. Another observation from the dynamical simulations is that after dissociation of the molecule the two H atoms remain adsorbed on the Pd cluster during the whole simulation, showing no tendency to spilling over the carbon substrate.

Activation barriers for the structural transition

The dynamical simulations presented in the previous Section reveal that the structure of the Pd_6 cluster anchored to a graphene vacancy is not immune to the dissociative chemisorption of H_2, and that this dissociation event induces a structural transformation in Pd_6@Gvac from the OCT to the IPB structure. In fact, previous static calculations showed that the IPB structure of Pd_6@Gvac with a dissociated hydrogen molecule is 0.22 eV more stable than the OCT structure with a dissociated molecule.[31] In addition, the adsorption sites of the two H atoms on the OCT and IPB structures of anchored Pd_6 are different. Evidently, the structural transformation is possible because the energy released on the dissociation of the H_2 molecule allows surpassing the activation barriers. To gain deeper insight on the isomerization transition we have performed static calculations of the activation barriers. For this purpose, the whole process is separated in two steps, focusing first on the energetics of the isomerization step exclusively. Therefore, in order to obtain activation energy barriers for the structural transformation (leaving aside the diffusion of the H atoms on the surface of the cluster, which will be tackled in a second step) we have considered transformations of anchored Pd_6 from OCT to IPB in which the two H atoms of the dissociated molecule are placed in similar adsorption sites in both isomeric structures. Two different methods to calculate a minimum energy path (MEP) have been considered. The first method consists in a step-wise constrained minimization to calculate the MEP for the isomerization from OCT to IPB when the H atoms are placed one on a face and the other on a lateral Pd-Pd edge (not belonging to the same face) of the upper square pyramid of the OCT structure and on two non-adjacent faces of the upper pyramid of the IPB structure (see Fig. 5). Notice that this last configuration is the ground state of dissociated H_2 on Pd_6@Gvac (see Fig. 1).

The MEP is as follows. First, the distance between the two Pd atoms of the breaking bond increases by about 30%. Those are the two Pd atoms supported on the graphene layer and labelled Pd_1 and Pd_2 in Fig. 1. Those two atoms have been marked in light blue color in Fig. 5. This initial bond elongation corresponds to steps 1 to 14 in Fig. 5, where the reaction

coordinate chosen is the distance between those two Pd atoms. During the elongation steps the two Pd atoms remain attached, respectively, to two opposite C-C bonds of one of the hexagons around the vacancy, and the activation barrier for the elongation of the Pd-Pd bond is quite small, 0.012 eV. Then the Pd_1-Pd_2 distance increases further as the Pd_2 atom moves to a neighbor bridge position on top of a C-C bond of an adjacent hexagon. This occurs in steps 14 to 24 in Fig. 5, where the reaction coordinate now corresponds to the set of (x, y) coordinates of the Pd_2 atom. There is a small activation barrier of 0.12 eV associated to the displacement of the Pd_2 atom on the graphene surface. Finally, in steps 24 to 29 of Fig. 5, in which the reaction coordinate is again the distance d(Pd_1-Pd_2), the Pd_1-Pd_2 bond breaks and the structure of the Pd cluster flattens, giving rise to the IPB structure.

A second MEP has been generated to study the OCT to IPB transformation, using the nudged elastic band (NEB) methodology.[44] In this case, we start from a low energy configuration of the Pd_6 octahedron and a dissociated hydrogen molecule having one H atom attached to a lateral Pd–Pd edge and the other H atom above the upper triangular face of the octahedron (see Fig. 6). That is, the starting configuration is different from that used to calculate the MEP of Fig. 5. The calculated magnitude of the activation energy barrier for the isomerization transition along this NEB path is 0.25 eV. This is the energy necessary to break the Pd–Pd bond between the two Pd atoms supported on the graphene layer (those two atoms are marked in light blue color in Fig. 6) and to re-accommodate the Pd cluster on the graphene surface. The distance between the two Pd atoms after breaking the bond is 4.48 Å. The adsorption sites of the two H atoms in the final configuration are the upper triangular face of the IPB and a lateral face of the upper pyramid adjacent to the first one, respectively. However, those adsorption positions do not correspond to the lowest energy configuration of the two H atoms on the IPB Pd_6@Gvac. Therefore, the H atoms have to diffuse on the surface of Pd_6 to reach the lowest energy configuration. To investigate this step we have calculated, using the NEB methodology, the minimum energy path for diffusion of one H atom from its adsorption site in the final configuration of the

previous MEP shown in Fig. 6, that is, from above the upper triangular face of the IPB structure, to the adsorption site corresponding to the ground state structure of dissociated hydrogen on Pd_6@Gvac. Along this path, H diffusion takes place in the IPB structure. The corresponding MEP is shown in Fig. S2 of the Supporting Material. A low barrier of only 0.04 eV is found for the diffusion of H atoms on the surface of the IPB Pd_6 cluster. The diffusion of the H atoms takes place between adjacent triangular faces of the IPB structure. The H atom moves from one face to above the common Pd-Pd edge of the two faces and then to the second face. Let us stress that the H atom does not penetrate inside the Pd_6 cluster along its diffusion path, but it remains on the surface of the cluster.

The calculated minimum energy paths for the processes leading to the structural transformation of Pd_6 upon the dissociative adsorption of H_2 exhibit relatively low activation barriers. Those barriers are much smaller than the energy released in the adsorption and dissociation of H_2 on the OCT structure of Pd_6@Gvac (0.76 eV and 0.24 eV, respectively, giving a total of 1.0 eV). These values, then, provide full support for the results obtained in the dynamical simulations. The adsorption and dissociation of H_2 take place on the OCT structure of Pd_6@Gvac and release a substantial amount of energy. Then it takes some time for the energy released to be channeled into the appropriate Pd–Pd bond, whose break up leads to the structural transformation from OCT to IPB. Most trajectories exhibiting the dissociation of the hydrogen molecule also display the structural transformation and end up in the ground state configuration (IPB) of dissociated H_2 on Pd_6@Gvac. Thus, the structural transformation takes place because it is both thermodynamically (more stable) and kinetically (low barriers) favored.

For comparison, and to better understand the effect of the graphene support on the structural transformation of Pd_6 upon dissociation of a hydrogen molecule, we have also investigated minimum energy paths for the structural transformation of free Pd_6 without and with dissociated H_2. The results are included in the Supporting Material. The barriers for the structural transformation in these two cases, 0.29 eV and 0.20 eV respectively, are

not too different from the barrier for the transformation in the supported cluster, the crucial difference being that the IPB is less stable than the OCT structure both in free Pd_6 and free Pd_6 with two chemisorbed H atoms.

Finally, we consider meaningful to analyze also how the electronic charge changes in the dissociation process. Some transfer of electronic charge is associated to the interaction between the hydrogen atoms and Pd_6. The charge transfer is very small in the case of molecular adsorption of H_2, in which case the Mulliken charges on the H atoms and neighbor Pd atoms are below 0.1 e. In contrast, the charges are larger in the case of dissociative adsorption. Table S1 of the Supplementary Information, giving the Mulliken charges on the different atoms, shows that the H atoms gain electronic charge from the Pd atoms. Each H atom gains about 0.3 electrons. The transferred electronic charge populates the antibonding state of the H_2 molecule and is responsible of the dissociation of the molecule. On the other hand, those Mulliken charges have very similar values before and after the transformation of the anchored Pd_6 from the OCT to the IPB structure.

Summary and conclusions

Ab initio dynamical simulations of the adsorption of molecular hydrogen on a Pd_6 cluster anchored to a graphene vacancy have been performed using density functional theory. Two hundred simulations were run, equally split in two groups with the Pd_6@Gvac substrate initially equilibrated at T=0 K and T=300 K, respectively. In all cases the molecules impinge normal to the graphene layer with an initial kinetic energy of 0.125 eV. The simulations lead to different possible outcomes. In most cases, the molecules are scattered back after colliding with either the Pd cluster or the graphene layer. A second outcome is that the H_2 is adsorbed on the Pd cluster. This occurs in 18% and 13% of the simulations starting at initial substrate temperatures T=0 K and T=300 K, respectively. Afterwards, one third of the adsorbed molecules undergo dissociation in a short time of less than 2 ps in the simulations at T=0 K,

and the two H atoms form chemisorption bonds with the Pd cluster. For the simulations at T=300 K, the proportion increases to 50 per cent. In general, H_2 dissociation triggers an isomerization transition of the anchored Pd_6 from its original octahedral structure into an incomplete pentagonal bipyramid (in which a Pd atom is missing from the equatorial plane of the bipyramid). The mechanism consists in the elongation and subsequent breaking of a Pd–Pd bond in the equatorial plane of the octahedron. This suggests that the activation energy barriers for that structural transition, which drives the system to its lowest energy state, are quite small and this has been further confirmed by static calculations. The relevant conclusion is that dissociation of H_2 on a metallic cluster supported on a carbon material can change the structural conformation of the metallic cluster. Although our result comes from a particular cluster and a specific reaction –this one occurring, for instance, in the anode of hydrogen fuel cells– the observation of a structural change, which means that the cluster structure is not immune to the reaction taking place on the cluster surface, may be relevant for many catalytic processes occurring on the surface of small metal particles.

Acknowledgement

Work supported by Junta de Castilla y León (Grant VA021G18), University of Valladolid (Grupo de Física de Nanoestructuras), Gobierno Vasco-UPV/EHU project IT756-13, and Spanish Ministerio de Economía y Competitividad (Grant No. FIS2016-76471-P). A. G. acknowledges a predoctoral fellowship from Junta de Castilla y León. The authors thankfully acknowledge the facilities provided by Centro de Proceso de Datos-Parque Científico (University of Valladolid) and by the DIPC computing center.

Supporting Information Available

Supporting Information: additional figures on the AIMD and MEP calculations.

References

(1) Alonso, J. A. *Structure and properties of atomic nanoclusters*, 2nd ed.; Imperial College Press: London, 2012.

(2) Alonso, J. A. Electronic and atomic structure, and magnetism of transition-metal clusters. *Chem. Rev.* **2000**, *100*, 637–677.

(3) Kohn, W.; Sham, L. J. Self-Consistent Equations Including Exchange and Correlation Effects. *Phys. Rev.* **1965**, *140*, A1133–A1138.

(4) Wales, D. J.; Doye, J. P. K. Global Optimization by Basin-Hopping and the Lowest Energy Structures of Lennard-Jones Clusters Containing up to 110 Atoms. *J. Phys. Chem. A* **1997**, *101*, 5111–5116.

(5) Kirkpatrick, S.; Gelatt, C. D.; Vecchi, M. P. Optimization by Simulated Annealing. *Science* **1983**, *220*, 671–680.

(6) Baletto, F.; Ferrando, R. Structural properties of nanoclusters: Energetic, thermodynamic, and kinetic effects and colescence of clusters. *Rev. Mod. Phys.* **2005**, *77*, 371–423.

(7) DiPaola, C.; Baletto, F. Chemical order and magnetic properties in small $M_{x-2}N_2$ nanoalloys. *Eur. Phys. J D* **2013**, *67*, 49.

(8) Baletto, F. Structural properties of sub-nanometer metallic clusters. *J. Phys.: Condens. Matter* **2019**, *31*, 113001.

(9) Mariscal, M.; Dassie, S.; Leiva, E. Collision as a way of forming bimetallic nanoclusters of various structures and chemical compositions. *J. Chem. Phys.* **2005**, *123*, 184505.

(10) Castro, A.; Marques, M. A. L.; Alonso, J. A.; Bertsch, G. F.; Yabana, K.; Rubio, A. Can optical spectroscopy directly elucidate the ground state of C_{20}? *J. Chem. Phys.* **2002**, *116*, 1930–1933.

(11) Li, X.; Wang, L.-S. Experimental search and characterization of icosahedral clusters: $Al_{12}X^-$ ($X = C, Ge, Sn, Pb$). *Phys. Rev. B* **2002**, *65*, 153404.

(12) Lyon, J. T.; Gruene, P.; Fielicke, A.; Meijer, G.; Janssens, E.; Claes, P.; Lievens, P. Structures of Silicon Cluster Cations in the Gas Phase. *J. Am. Chem. Soc.* **2009**, *131*, 1115–1121.

(13) Marcos, P. A.; Alonso, J. A.; Rubio, A.; López, M. J. Simulating the thermal stability and phase changes of small carbon clusters and fullerenes. *Eur. Phys. J. D* **1999**, *6*, 221–233.

(14) DiPaola, C.; Pavan, L.; D'Agosta, R.; Baletto, F. Structural stability and uniformity of magnetic Pt_{13} nanoparticles in NaY zeolite. *Nanoscale* **2017**, *9*, 15658.

(15) Bumüller, D.; Hehn, A.-S.; Waldt, E.; Ahlrichs, R.; Kappes, M.; Schooss, D. Ruthenium Cluster Structure Change Induced by Hydrogen Adsorption: Ru_{19}. *J. Phys. Chem. C* **2017**, *121*, 10645–10652.

(16) Heiz, U.; Landman, U. *Nanocatalysis*; Imperial College Press: Berlin, 2005.

(17) Haruta, M. Size- and support-dependency in the catalysis of gold. *Catalysis Today* **1997**, *36*, 153–166.

(18) Zemichael, F. W.; Tikhov, A. P. M. S.; Lambert, R. M. Propene Epoxidation over K-Promoted $Ag/CaCO_3$ Catalysts: The Effect of Metal Particle Size. *Catal. Lett.* **2002**, *80*, 93–98.

(19) *EG & G Technical Services, Fuel cell handbook*, 7th ed.; U.S. Dept. of Energy, Office of Fossil Energy, National Energy Technology Laboratory Morgantown, WV , 2004.

(20) Antolini, E. Palladium in fuel cell catalysis. *Energy Environ. Sci.* **2009**, *2*, 915–931.

(21) Adams, B. D.; Chen, A. The role of palladium in a hydrogen economy. *Mater. Today* **2011**, *14*, 282 – 289.

(22) Züttel, A. Materials for hydrogen storage. *Mater. Today* **2003**, *6*, 24–33.

(23) Alonso, J. A.; Cabria, I.; López, M. J. Simulation of hydrogen storage in porous carbons. *J. Mater. Res.* **2013**, *28*, 589–604.

(24) Gogotsi, Y.; Dash, R. K.; Yushin, G.; Yildirim, T.; Laudisio, G.; Fischer, J. E. Tailoring of Nanoscale Porosity in Carbide-Derived Carbons for Hydrogen Storage. *J. Am. Chem. Soc.* **2005**, *127*, 16006–16007.

(25) Contescu, C. I.; Brown, C. M.; Liu, Y.; Bhat, V. V.; Gallego, N. C. Detection of Hydrogen Spillover in Palladium-Modified Activated Carbon Fibers during Hydrogen Adsorption. *J. Phys. Chem. C* **2009**, *113*, 5886–5890.

(26) Bhat, V. V.; Contescu, C. I.; Gallego, N. C.; Baker, F. S. Atypical Hydrogen Uptake on Chemically Activated, Ultramicroporous Carbon. *Carbon* **2010**, *48*, 1331–1340.

(27) Contescu, C. I.; van Benthem, K.; Li, S.; Bonifacio, C. S.; Pennycook, S. J.; Jena, P.; Gallego, N. C. Single Pd Atoms in Activated Carbon Fibers and their Contribution to Hydrogen Storage. *Carbon* **2011**, *49*, 4050–4058.

(28) Zielinska, B.; Michalkiewicz, B.; Chen, X.; Mijowska, E.; Kalenczuk, R. J. Pd supported ordered mesoporous hollow carbon spheres OMHCS for hydrogen storage. *Chem. Phys. Lett.* **2016**, *647*, 14 – 19.

(29) Hao, L.; Liu, Y.; Du, Y.; Chen, Z.; Han, Z.; Xu, Z.; Zhu, J. Highly Enhanced H_2 Sensing Performance of Few-Layer $MoS_2/SiO2_2/Si$ Heterojunctions by Surface Decoration of Pd Nanoparticles. *Nanoscale Res. Lett.* **2017**, *12*, 567.

(30) Li, J.; Fan, R.; Hu, H.; Yao, C. Hydrogen sensing performance of silica microfiber elaborated with Pd nanoparticles. *Materials Lett.* **2018**, *212*, 211–213.

(31) Granja, A.; Alonso, J. A.; Cabria, I.; López, M. J. Competition between Molecular and

Dissociative Adsorption of Hydrogen on Palladium Clusters Deposited on Defective Graphene. *RSC Advances* **2015**, *5*, 47945–47953.

(32) Kresse, G.; Furthmüller, J. Efficiency of ab-initio total energy calculations for metals and semiconductors using a plane-wave basis set. *Compt. Mater. Sci.* **1996**, *6*, 15 – 50.

(33) Kresse, G.; Hafner, J. Ab initio molecular dynamics for liquid metals. *Phys. Rev. B* **1993**, *47*, 558–561.

(34) Perdew, J. P.; Chevary, J. A.; Vosko, S. H.; Jackson, K. A.; Pederson, M. R.; Singh, D. J.; Fiolhais, C. Atoms, molecules, solids, and surfaces: Applications of the generalized gradient approximation for exchange and correlation. *Phys. Rev. B* **1992**, *46*, 6671–6687.

(35) Blanco-Rey, M.; Juaristi, J. I.; Alducin, M.; López, M. J.; Alonso, J. A. Is Spillover Relevant for Hydrogen Adsorption and Storage in Porous Carbons Doped with Palladium Nanoparticles? *J. Phys. Chem. C* **2016**, *120*, 17357–17364.

(36) López, M. J.; Cabria, I.; Alonso, J. A. Palladium Clusters Anchored on Graphene Vacancies and Their Effect on the Reversible Adsorption of Hydrogen. *J. Phys. Chem. C* **2014**, *118*, 5081–5090.

(37) Cabria, I.; López, M. J.; Fraile, S.; Alonso, J. A. Adsorption and Dissociation of Molecular Hydrogen on Palladium Clusters Supported on Graphene. *J. Phys. Chem. C* **2012**, *116*, 21179–21189.

(38) Blöchl, P. E. Projector augmented-wave method. *Phys. Rev. B* **1994**, *50*, 17953.

(39) Kresse, G.; Joubert, D. From ultrasoft pseudopotentials to the projector augmented-wave method. *Phys. Rev. B* **1999**, *59*, 1758–1775.

(40) Monkhorst, H. J.; Pack, J. D. Special points for Brillouin-zone integrations. *Phys. Rev. B* **1976**, *13*, 5188–5192.

(41) Methfessel, M.; Paxton, A. T. High-precision sampling for Brillouin-zone integration in metals. *Phys. Rev. B* **1989**, *40*, 3616–3621.

(42) DACAPO. `https://wiki.fysik.dtu.dk/dacapo`, Last accessed 04-09-2018.

(43) Vanderbilt, D. Soft self-consistent pseudopotentials in a generalized eigenvalue formalism. *Phys. Rev. B* **1990**, *41*, 7892–7895.

(44) Henkelman, G.; Jóhannesson, G.; Jónsson, H. *Progress on Theoretical Chemistry and Physics*; Kluwer Academic, 2000; Chapter 10. Methods for Finding Saddle Points and Minimum Energy Paths.

(45) Nosé, S. A unified formulation of the constant temperature molecular dynamics methods. *J. Chem. Phys.* **1984**, *81*, 511–519.

(46) Groß, A.; Dianat, A. Hydrogen Dissociation Dynamics on Precovered Pd Surfaces: Langmuir is Still Right. *Phys. Rev. Lett.* **2007**, *98*, 206107.

(47) Nattino, F.; Díaz, C.; Jackson, B.; Kroes, G.-J. Effect of Surface Motion on the Rotational Quadrupole Alignment Parameter of $\mathbf{D}_2$ Reacting on Cu(111). *Phys. Rev. Lett.* **2012**, *108*, 236104.

(48) Nattino, F.; Ueta, H.; Chadwick, H.; van Reijzen, M. E.; Beck, R. D.; Jackson, B.; van Hemert, M. C.; Kroes, G.-J. Ab Initio Molecular Dynamics Calculations versus Quantum-State-Resolved Experiments on CHD3 + Pt(111): New Insights into a Prototypical Gas Surface Reaction. *J. Phys. Chem. Lett.* **2014**, *5*, 1294–1299, PMID: 26269970.

(49) Kolb, B.; Guo, H. Communication: Energy transfer and reaction dynamics for DCl scattering on Au(111): An ab initio molecular dynamics study. *J. Chem. Phys.* **2016**, *145*, 011102.

(50) Novko, D.; Lončarić, I.; Blanco-Rey, M.; Juaristi, J. I.; Alducin, M. Energy loss and surface temperature effects in ab initio molecular dynamics simulations: N adsorption on Ag(111) as a case study. *Phys. Rev. B* **2017**, *96*, 085437.

(51) Zhou, X.; Kolb, B.; Luo, X.; Guo, H.; Jiang, B. Ab Initio Molecular Dynamics Study of Dissociative Chemisorption and Scattering of CO2 on Ni(100): Reactivity, Energy Transfer, Steering Dynamics, and Lattice Effects. *J. Phys. Chem. C* **2017**, *121*, 5594–5602.

(52) Zhou, L.; Jiang, B.; Alducin, M.; Guo, H. Communication: Fingerprints of reaction mechanisms in product distributions: Eley-Rideal-type reactions between D and CD3/Cu(111). *J. Chem. Phys.* **2018**, *149*, 031101.

(53) Füchsel, G.; Zhou, X.; Jiang, B.; Juaristi, J. I.; Alducin, M.; Guo, H.; Kroes, G.-J. Reactive and Nonreactive Scattering of HCl from Au(111): An Ab Initio Molecular Dynamics Study. *J. Phys. Chem. C* **2019**, *123*, 2287–2299.

(54) López, M.; Blanco-Rey, M.; Juaristi, J. I.; Alducin, M.; Alonso, J. A. Manipulating the Magnetic Moment of Palladium Clusters by Adsorption and Dissociation of Molecular Hydrogen. *J. Phys. Chem. C* **2017**, *121*, 20756–20762.

(55) Humphrey, W.; Dalke, A.; Schulten, K. VMD – Visual Molecular Dynamics. *Journal of Molecular Graphics* **1996**, *14*, 33–38.

Graphical TOC Entry

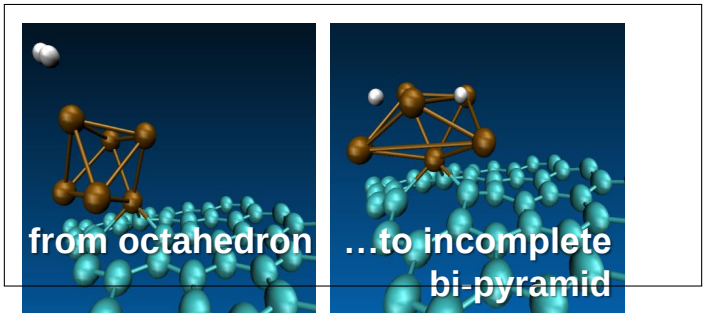

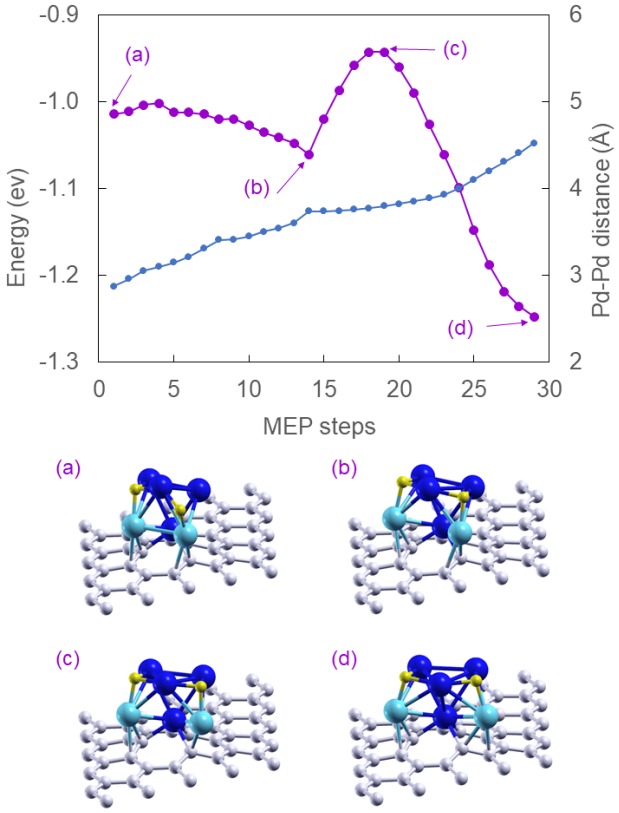

Figure 5: Minimum energy path for the transformation from OCT to IPB of Pd_6@Gvac with one dissociated hydrogen molecule. The H atoms occupy similar adsorption sites in the initial and final configurations. The initial configuration has one H atom adsorbed on a face and the other on a lateral Pd-Pd edge of octahedral Pd_6@Gvac, and the final configuration is the ground state structure of the system formed by two H atoms adsorbed on Pd_6@Gvac. The isomerization path has been calculated using a constrained minimization procedure, as explained in detail in the text. The purple curve (left axis) gives the energy along the path. The zero energy reference is formed by the free H_2 molecule and the lowest energy configuration (OCT) of Pd_6@Gvac. The blue curve (right axis) gives the distance between the two Pd atoms of the bond that breaks in the structural transformation. Snapshots are shown for selected configurations along the path. The snapshots are labeled (a) through (d). The two Pd atoms of the breaking bond are colored in light blue.

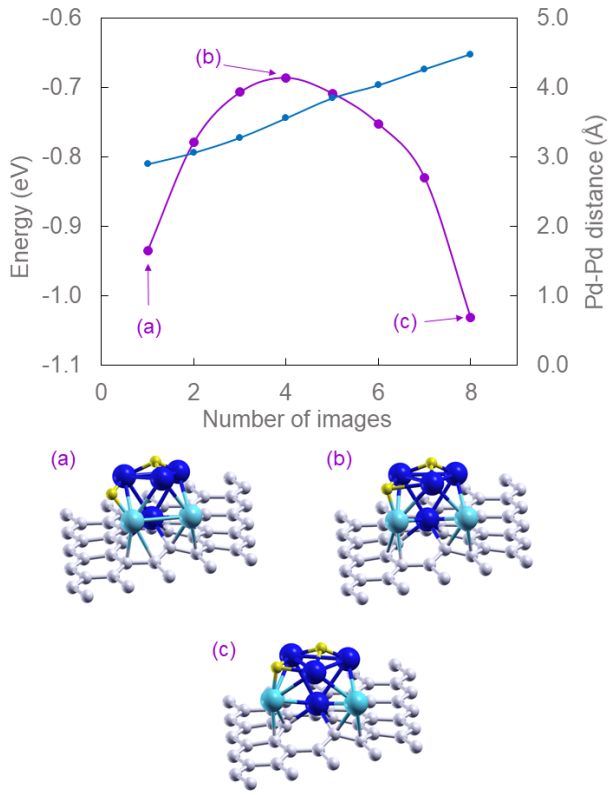

Figure 6: Minimum energy path for the transformation from OCT to IPB of Pd_6@Gvac with one dissociated hydrogen molecule. The initial structure is a low energy configuration of dissociated H_2 on OCT Pd_6 (see text for details). The purple curve (left axis) gives the energy along the path, calculated using the NEB methodology. A zero energy reference is taken formed by the free H_2 molecule and the lowest energy configuration (OCT) of Pd_6@Gvac. The blue curve (right axis) gives the Pd–Pd distance of the bond that breaks in the structural transformation. Snapshots of selected configurations along the path are given. The snapshots are labeled (a) through (c). The two Pd atoms of the breaking bond are colored in light blue.